Controlled Source Electromagnetic (CSEM) technique for detection and delineation of hydrocarbon reservoirs: an evaluation

Kurang Mehta, Misac Nabighian and Yaoguo Li, Center for Gravity, Electrical & Magnetic Studies, Colorado School of Mines; Doug Oldenburg, UBC-GIF, University of British Columbia.*

Summary

The resolving capabilities of marine Controlled Source Electromagnetic technique are evaluated on various theoretical models of finite lateral extent, both horizontal and dipping. We analyze the effects of variable bathymetry and of salt underlying the targets, and also present novel ways of displaying data for multiple transmitter-receiver locations.

Introduction

The marine Controlled Source Electromagnetic technique was developed almost three decades ago to study the conductivity structure beneath the seafloor. An exhaustive and still valid treatment of the CSEM techniques can be found in Chave et al. (1991). One advantage of sub-sea measurements is that the highly conductive sea (approximately 3.2 S/m) acts as a low pass filter for fluctuating EM fields generated above it either in the ionosphere or magnetosphere. At frequencies as low as 1 Hz, a few hundred meters of water will practically completely eliminate the effect of above-water EM sources including the man-made ones or those due to cultural noises. As a result weak electromagnetic fields that propagate in the underlying sediments from a sea-bottom artificial source are measurable at large transmitter-receiver separations of the order of kilometers.

Recently the marine CSEM technique was applied commercially to the problem of detecting the presence of hydrocarbon filled layers in the sub-sea formations (Eidesmo et al., 2002) and a number of companies are now providing this service. The marine CSEM technique for remote and direct identification of hydrocarbon filled layers in deepwater areas uses a mobile horizontal electric dipole (HED) source, located slightly above the sea-floor, and an array of electric and magnetic dipole field receivers located directly on the seafloor. Most of the measurements are done in frequency-domain, using low frequencies around 1 Hz, although there are compelling reasons why such measurements would yield better results if carried out and interpreted in time-domain.

1D models

Most of the published work to date dealt with simple 1D models investigating the diffusion of EM signals through either a simple two-layer structure, representing the sea and the sub-sea, or a four-layer structure which incorporates a thin, higher resistivity hydrocarbon filled layer (Figure 1). Following Eidesmo et al. (2002) we present in figure 2a the calculated responses, for different frequencies, over the two models shown in figure 1 while in figure 2b we present the normalized response i.e. the four-layer response divided by the two-layer response. The relative increase in signal strength in the presence of a resistive layer is obvious and becomes more prominent with larger sea depths. Noteworthy is also the presence of the *air-wave* (i.e. the signal that travels from the transmitter to the sea surface, then along the sea-air boundary and then back to the sea-floor receivers) which manifests as a break in slope around 3.5 km transmitter-receiver separation.

Equivalency principle

Similar to other electrical methods CSEM is also affected by the *equivalency principle*, i.e. the response depends, within limits, primarily on the transverse resistance of the target (resistivity thickness product) and not on the individual values of resistivity and thickness. Figure 3 shows the calculated curves for three different cases of four-layer models, each having a transverse resistance of 10,000 ohms. As can be easily seen the three responses are practically identical.

Models with finite lateral extent

An infinitely extent layer is a first approximation of a real case. Figure 4 shows a 2D model in which the hydrocarbon filled layer has a finite lateral extent of 13 km and thickness of 150 m. This model will allow us to evaluate more realistically under what conditions (i.e. depth below seafloor, frequency, transverse resistance, etc) can such a thin layer be detected. We use a finite-volume based 3D modeling code developed at UBC-GIF (Haber, et al, 2001) to carry out the calculation for this and subsequent models. The calculated response for a transmitter located over the body center is shown in figure 4 while the case for a transmitter located outside the body is shown in figure 5. Their respective normalized responses are shown in figure 6. We conclude that, for a centrally located transmitter, the radial electric field can detect both the presence of a hydrocarbon filled layer and the location of its edges. For off-centered transmitter locations only the existence of the resistive layer can be inferred from the normalized curve although the farthest edge can be determined from the radial field itself. The problem becomes more complicated if the bathymetry varies appreciably.

Data presentation

Figures 4 and 5 give the expected responses for two fixed transmitter locations and for in-line located

receivers. For a typical array of receivers located over the target at the bottom of the sea a common way of presenting data is through contour plots (or images) of the measured quantities (figure 7).

In actual field conditions the transmitter is continuously moving and data has to be presented differently. One approach is to show the data in a plane with transmitter location on the Y axis and receiver location on the X axis (Tx-Rx plot). For the two-layer case shown in figure 1 the Tx-Rx plot is shown in figure 8a while the four-layer case is shown in figure 8b. The spotty nature of these plots is explained by the discrete nature of transmitter and receiver locations (2 km separation for transmitters and 1 km separation for receivers). The departure between the two plots is significant and the inflated portions of the plot in figure 8b can give indications on target extent. The edges of the resistive layer are shown by two arrows. Normalizing figure 8b results by figure 8a results yields additional information but, due to space limitations, will not be presented here

Another way of presenting data simultaneously for all transmitter and receiver locations is to present values of the radial electric field as a pseudo-section, similar to the ones used in the DC resistivity / IP method. The pseudo-section plot for this case is shown in figure 9. The resistive target is located between -6500 and 6500 m. The transmitters are located between -11500 and 11500 m and the receivers extend from -16500 to 16500 m. The pseudo-section pattern is similar with the pattern seen over the same target in the DC resistivity / IP method, i.e. pant-legs anomalies (or Chevron type anomalies) surrounded by lows, both inside and outside the region of high resistivity values.

Dipping layer

It is interesting to look now at the response over a dipping resistive layer and see if we can detect its extent and also get some indication of the direction of its dip. The model shown in figure 10 has a resistive layer dipping 2.2 degrees with respect to the horizontal. The response of the electric field shows two breaks indicating both edges of the layer. The interesting observation is that, not unexpectedly, the break over the shallower edge occurs at slightly higher amplitude than the break over the deeper edge. This implies that, at least theoretically, the CSEM technique can indicate the dip direction for the case of a dipping resistive layer.

Salt body

As seen before the air-wave manifests itself as a clear break in the observed curve (figure 2a). The question arises if a high resistivity salt formation will also yield a similar type of signal.

First we look at the effect of increasing the resistivity of the thin resistive layer from 100 ohm-m to 10,000 ohm-m, typical of the resistivity of salt. As seen from figure 11a the response changes dramatically both in amplitude and in character. When compared with the two-layer curve shown in the same graph we notice that the salt layer response has a pattern similar to air-wave. In other words, due to the high resistivity contrast, a signal similar to air wave is also coming from the top of the salt. To further prove the existence of this *salt-wave* we increased the thickness of salt layer to 5 km with the results shown in figure 11b. Two conclusions can be reached by examining these plots. First, not unexpectedly, the thick salt gave a lower amplitude response than the thinner salt, i.e. it does not have the same signal transmission and guiding capability. This implies that there is an optimum salt thickness for which the response and hence signal transmission will be maximum. Second, the response for the thick salt, except for amplitude, is similar in character to the response for the two layer case, further proving the existence of a *salt-wave* similar in character to air-wave.

Bathymetry effect

Bathymetry plays a key role on the measured response and an accurate evaluation of its contribution is essential in the interpretation process. Usually the bathymetry response and the response from a buried resistive target have different wavelengths which might facilitate their separation with accurate modeling. Could a bathymetric high in sub-sea topography be mistaken for a buried resistive target? Figure 12a shows a simple model of a hill on the sea-floor with a 6.5 km lateral extent and a height of 690 meters. The response over the hill is shown in figure 12b along with the response for two-layers (flat bathymetry) and for four-layers (i.e. including a sub-sea resistive layer). There is a disturbingly close resemblance between the response of a bathymetry high and the response from a buried resistive layer. Although a quantitative interpretation such as inversion may distinguish between these two scenarios, they will certainly not be distinct to visual inspection in actual field conditions.
Hence, it is crucial to know and be able to calculate the effect of the bathymetry before attempting any interpretation of CSEM data.

Acknowledgements

Support for this work was provided by Chevron-Texaco, Conoco-Phillips, Marathon and Total.

References

Chave, A.D., Constable, S.C., Edwards, R.N., 1991, Electrical Exploration Methods for the Seafloor, in Electromagnetic Methods in Applied Geophysics, M. Nabighian (ed), SEG

E. Haber and U. Ascher, 2001, Fast finite volume simulation of 3D electromagnetic problems with

highly discontinuous coefficients. SIAM J. Scientific Computing, **22**, 1943--1961:

Eidesmo, T., Ellingsrud, S., MacGregor, L.M., Constable, S., Sinha, M.C., Johansen, S., Kong, F.N., Westerdahl, H., 2002, Sea Bed Logging (SBL), a new method for remote and direct identification of hydrocarbon filled layers in deepwater areas, First Break, v.20.3

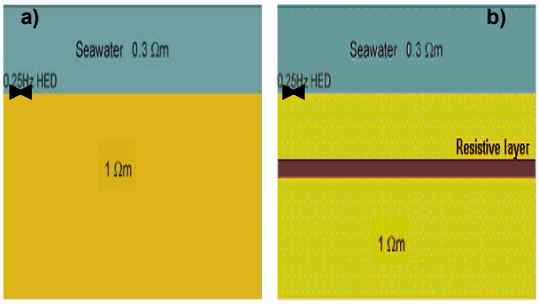

Figure 1. Figure (a) shows the two-layer case (sea and sub-sea). Figure (b) shows the four-layer case incorporating a resistive layer situated 1000 m below sea-floor, having a thickness of 100 meters and a resistivity of 100 ohm-m. The sea depth is 1 km. and the transmitter frequency is 0.25 Hz.

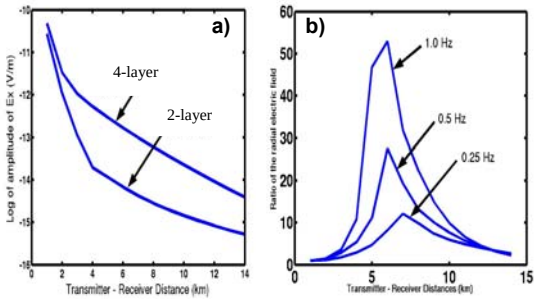

Figure 2. (a) Calculated radial electric field obtained over the two models shown in figure 1; (b) the normalized response for variable frequencies. Sea depth is 1 km.

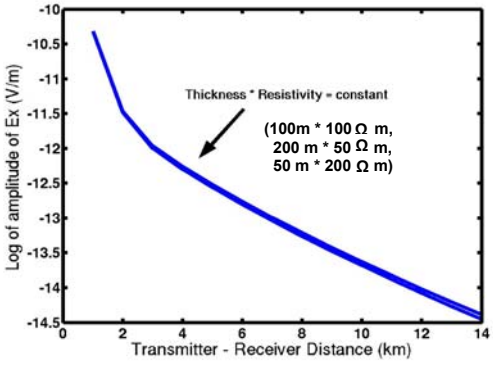

Figure 3. Response of the radial electric field for three different resistivity thickness combinations having the same transverse resistance.

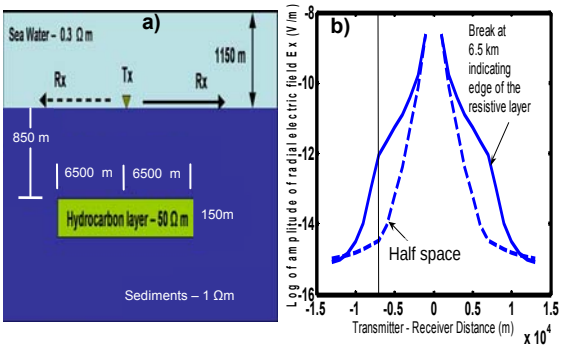

Figure 4. Model showing a resistive layer of 13 km lateral extent and the response of the radial electric field for a centrally located transmitter. The breaks in slope in the response give clear indications of the edges of the resistive layer.

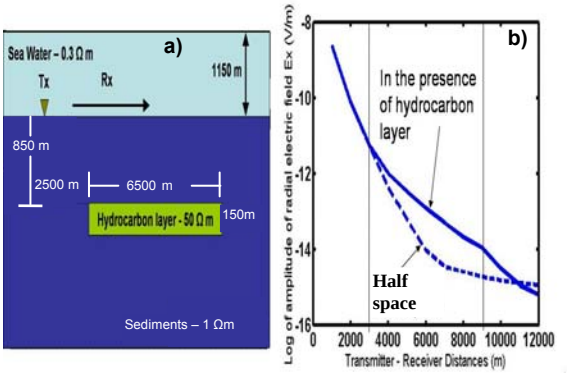

Figure 5. Response of the radial electric field for a source located 2.5 km leftward from the left edge. The breaks in slope in the response give indication of the two edges of the resistive layer.

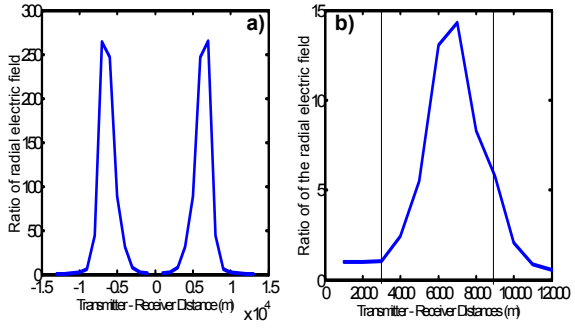

Figure 6. (a) Response of the radial electric field for the model shown in figures 4 normalized by the two-layer response. The highs in the response give clear indication of the edges of the resistive layer. (b) Same for model 5.

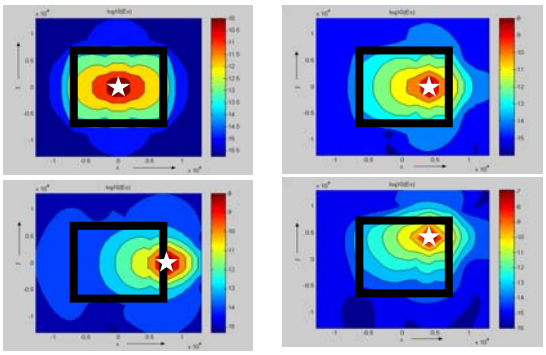

Figure 7. Plan view of radial electric field image over a square 13km resistive plate of thickness 150 m and located at a depth of 850 m. The black boundary shows the plate extent and the white star indicates the source location.

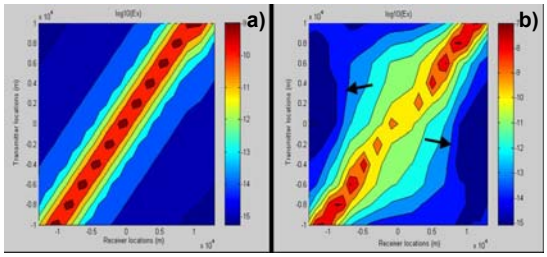

Figure 8. (a) Response of the radial electric field for the two layer case; (b) same for the four-layer model shown in figure 4. The receivers are placed every 1 km and the transmitter is moved in steps of 2 km to minimize calculations.

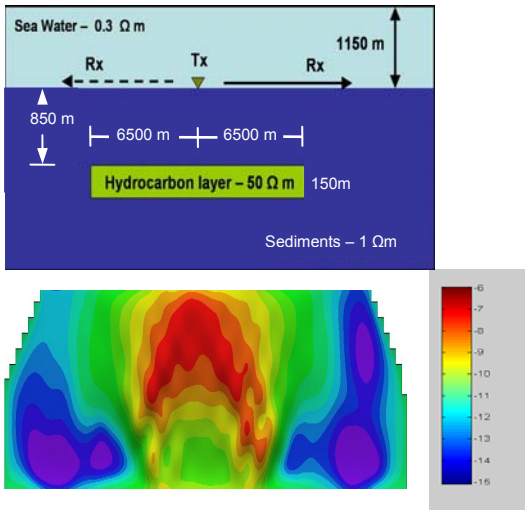

Figure 9. Pseudo-section above a resistive layer

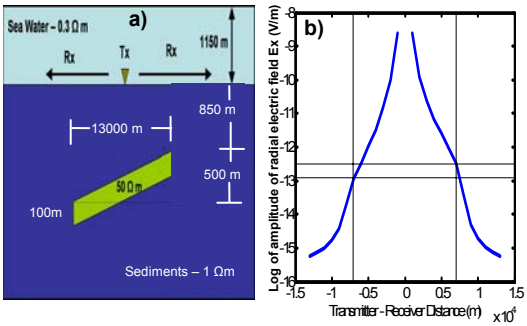

Figure 10. Response of the radial electric field for a dipping layer. The breaks in the response help indicate the direction of tilt of the layer.

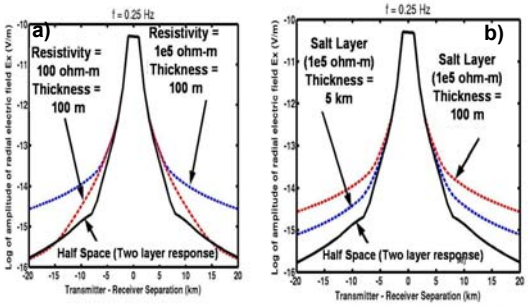

Figure 11. (a) 100 meter thick layer response having resistivities of 100 ohm-m and 10,000 ohm-m (salt) compared with the two layer response; (b) 100 meter and 5 km thick salt response compared with the two layer response. The sea depth is 1.15 km and layers are located at a depth of 2 km.

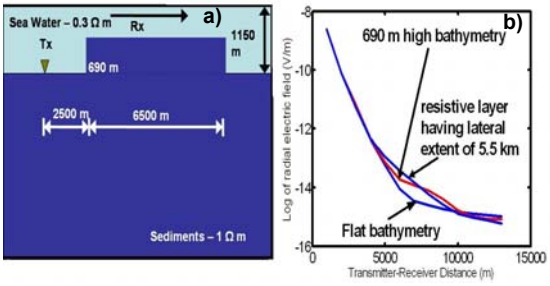

Figure 12. (a) Model showing the two layer case with a rise of 690 m elevation. The rise has a lateral extent of 6.5 km. (b) The radial electric field response for a 5.5 km resistive layer compared with the response from the rise and from a flat bathymetry.